ORIGINAL ARTICLE

Combination of AAV-delivered tumor suppressor PTEN with anti-PD-1 loaded depot gel for enhanced antitumor immunity

Yongshun Zhang[a], Lan Yang[a], Yangsen Ou[a], Rui Hu[a], Guangsheng Du[a], Shuang Luo[a], Fuhua Wu[a], Hairui Wang[a], Zhiqiang Xie[a], Yu Zhang[a], Chunting He[a], Cheng Ma[a], Tao Gong[a], Ling Zhang[b], Zhirong Zhang[a], Xun Sun[a,*]

[a]Key Laboratory of Drug-Targeting and Drug Delivery System of the Education Ministry and Sichuan Province, Sichuan Engineering Laboratory for Plant-Sourced Drug and Sichuan Research Center for Drug Precision Industrial Technology, West China School of Pharmacy, Sichuan University, Chengdu 610041, China
[b]Med-X Center for Materials, College of Polymer Science and Engineering, Sichuan University, Chengdu 610065, China

Abstract Recent clinical studies have shown that mutation of phosphatase and tensin homolog deleted on chromosome 10 (PTEN) gene in cancer cells may be associated with immunosuppressive tumor microenvironment (TME) and poor response to immune checkpoint blockade (ICB) therapy. Therefore, efficiently restoring PTEN gene expression in cancer cells is critical to improving the responding rate to ICB therapy. Here, we screened an adeno-associated virus (AAV) capsid for efficient PTEN gene delivery into B16F10 tumor cells. We demonstrated that intratumorally injected AAV6-PTEN successfully restored the tumor cell PTEN gene expression and effectively inhibited tumor progression by inducing tumor cell immunogenic cell death (ICD) and increasing immune cell infiltration. Moreover, we developed an anti-PD-1 loaded phospholipid-based phase separation gel (PPSG), which formed an *in situ* depot and sustainably release anti-PD-1 drugs within 42 days *in vivo*. In order to effectively inhibit the recurrence of melanoma, we further applied a triple therapy based on AAV6-PTEN, PPSG$^{@anti-PD-1}$ and CpG, and showed that this triple therapy strategy enhanced the synergistic antitumor immune effect and also induced robust immune memory, which completely rejected tumor recurrence. We anticipate that this

triple therapy could be used as a new tumor combination therapy with stronger immune activation capacity and tumor inhibition efficacy.

1. Introduction

For the treatment of cancer, a single treatment method (radio-therapy, chemotherapy, immunotherapy, etc.) cannot achieve satisfactory therapeutic efficacy[1]. The combination of multiple therapies is a major trend in cancer treatment[2–4]. In recent years, the immune checkpoint inhibitor therapy that reactivates T cells by blocking the immune checkpoint pathway to achieve anti-tumor immunity has achieved great clinical success in treating cancer[5]. A series of inhibitors against immune checkpoints such as cytotoxic T lymphocyte-associated protein 4 (CTLA-4), pro-grammed cell death 1 (PD-1) and PD-1 ligand 1 (PD-L1) have been developed. However, there is evidence that more than two-thirds of patients are resistant to ICB therapy[6,7]. Studies have shown that this low response rate of ICB therapy is mainly caused by the immunosuppressive environment in tumor tissues[7,8]. Furthermore, ICB therapy requires multiple systemic doses, resulting in poor patient compliance and systemic adverse re-actions[9]. Developing new combination immunotherapy that can synergistically enhance immune activation and relieve immune suppression becomes an important challenge.

PTEN is a widely studied tumor suppressor, and the deletion of the PTEN gene has been observed in a variety of cancers[10]. Recent clinical studies have shown that the deficiency of PTEN gene expression is an important reason for the decreased immune cell infiltration in tumor tissues and higher resistance to anti-PD-1 therapy[11–14]. Further mechanism studies showed that PTEN can inhibit tumorigenesis by causing autophagy in tumor cells[15,16]. Autophagy in tumor cells may release damage-associated mo-lecular patterns (DAMPs), including adenosine triphosphate (ATP), high mobility frame 1 (HMGB1), heat shock proteins (HSP), and calreticulin (CRT) expressed on cell membranes[17–19]. These damage-associated molecular patterns can activate anti-tumor immunity in cancer therapy and increase the infiltration of immune cells in tumor tissues[20–22]. At the same time, tumor an-tigens produced by tumor cell death can be presented to T cells *via* mature dendritic cells (DC) for immune activation[22].

Based on the above findings, we speculate that PTEN gene restoration in tumor cells should improve the effect of ICB treatment, and these two therapies could have a synergistic anti-tumor effect. For PTEN therapy, it is crucial to safely and effi-ciently deliver the PTEN gene to tumor cells *in vivo*. The success of mRNA vaccines against COVID-19 showed the broad prospects of mRNA delivery[23,24] and also revealed the urgent challenges to be solved, including improving the infection efficiency of mRNA delivery vectors to host cells, decreasing potential inflammation side effects, and improving the stability of the mRNA delivery system[25]. AAV is an ideal vehicle for delivering the PTEN gene to tumor cells due to their advantages including high gene delivery efficiency, low immunogenicity, and high safety[26]. Clinically, AAV has been used for gene therapy of various diseases, such as ROCTAVIAN™, the recently approved AAV gene therapy for

hemophilia A. In addition, studies have shown that AAV has strong tumor penetration and therefore has the potential to effectively deliver PTEN genes into the tumors[27].

Tumor recurrence has become the main reason for treatment failure in malignant tumors[27,28]. For tumor recurrence, how to effectively activate the immune system and induce tumor-specific immune memory is very important. Tumor vaccines are an ideal approach to eradicate tumors by inducing tumor-specific cellular immunity as well as humoral immunity[28]. CpG, a Th1 immune adjuvant, is a TLR9 agonist and has potent immunostimulatory adjuvant activity[29]. Therefore, we speculate that the combination of the released tumor antigens induced by the restoration of the PTEN and immune adjuvants CpG may efficiently activate the immune system to form a long-term immune memory response.

To sum, in the current study, we combined AAV-based tumor suppressor gene delivery therapy, with ICB therapy and *in situ* tumor vaccine therapy to elicit a synergistic anti-tumor immune response. Our results showed that restoration of the PTEN gene induced tumor cell apoptosis and ICD. Moreover, we have developed an anti-PD-1 loaded phospholipid-based phase sepa-ration gel capable of forming anti-PD-1 drug depots *in vivo*. PPSG is composed of phospholipids (E80), soybean oil, and a small amount of ethanol. E80 has poor water solubility, but very high solubility in ethanol. After subcutaneous injection of PPSG around the tumor, ethanol rapidly diffuses into the surrounding tissues. The precipitation of E80 leads to an increase in system viscosity. In this way, PPSG in the sol state at the time of injection trans-formed into a semi-solid or solid gel *in situ* after injection. At the same time, we used CpG as an immune adjuvant of the "*in situ* tumor vaccine" in combination with the above two kinds of therapy to induce tumor-specific cellular immunity and humoral immunity. Finally, we evaluated the effect of this triple therapy in a melanoma model. The results showed that this triple therapy synergistically exerts anti-tumor immune effects and induces long-term immune memory in experimental animals, which effectively avoids tumor recurrence.

2. Materials and methods

2.1. Study design

The purpose of our study was to probe into whether and how the AAV-based restoration of tumor suppressor PTEN could achieve antitumor effects. Furthermore, we explored a synergistic tumor combination therapy, which is a triple therapy that combines AAV delivery of tumor suppressors, immune checkpoint inhibitor therapy, and immunotherapy to treat tumors.

We first screened the most efficient AAV serotype for B16F10 infection to deliver the PTEN gene and then assessed its trans-duction in melanoma cells by cell viability assays, apoptosis detection, immunofluorescence, and confocal imaging effects. For

mechanistic studies, we analyzed the induction of ICD of tumor cells *in vitro* ($n = 3$ replicates per group) and changes in the phenotype/number of immune cells *in vivo* ($n = 5$ mice per group) by flow cytometry, ELISA, and immunofluorescence imaging. We prepared a sustained-release gel to deliver anti-PD-1 and characterized the properties of this gel as well as the drug release behavior by small animal *in vivo* imaging and viscometer. To evaluate the effect of triple therapy in the treatment of melanoma, we used a subcutaneous mouse model of melanoma to analyze the effect of AAV-PTEN alone, the combination of any two treatments, and the combination of three treatments ($n = 10$ mice per group) antitumor effect. For mechanistic studies of the triple therapy, we analyzed the induction of ICD and changes in immune cell phenotype/number at tumor tissues, as well as changes in immune cell phenotype/number in the spleen ($n = 4$ mice per group) by flow cytometry, ELISA, and immunofluorescence. The animals were randomly assigned to unblinded treatment groups.

2.2. Plasmid, drugs, and antibodies

The three plasmid systems, including target gene plasmid (pAAV-CAG-mCherry), capsid plasmid (pAAV-6, pAAV-1, pAAV-7m8, pAAV-7, pAAV-8, pAAV-10) and helper plasmid (pHelper), were all purchased from Fenghui Biotechnology (Hunan, China). The complementary DNA (cDNA) encoding the mouse PTEN gene was synthesized from GENEWIZ (Suzhou, China). pAAV-CAG-PTEN was obtained by replacing mCherry gene in pAAV-CAG-mCherry with PTEN gene. Reverse the PTEN gene sequence in pAAV-CAG-PTEN to get pAAV-CAG-PTEN[R].

The anti-PD-1 used in this study is AUNP-12, a polypeptide purchased from Selleck (USA) with a purity of 99.20%. Cy5-AUNP-12 was purchased from Guoping pharmaceutical co (Anhui, China) with a purity of 90%. CpG was synthesized in GENEWIZ (Suzhou, China) with 90% purity.

Antibodies for Western blot (WB) and Immunofluorescence (IF): anti-mouse PTEN, CRT, β-actin and anti-rabbit FITC, CY3 fluorescent secondary antibodies were purchased from ABclonal Tech (Wuhan, China). Antibodies for flow cytometry test: CD11c-PE, CD80-FITC, CD86-APC, CD3-APC, CD8-FITC, CD4-APC-eflour780, CD69-PE, CD274-PE, CD11b-FITC, CD206-PE-Cy7, CD86-APC, IL-4-PE, IFN-γ-APC, TNF-α-eflour450, IL-2-PE5.5, CD4-APC-eflour780, CD44-APC, CD62L-PE were all purchased from Invitrogen (USA).

2.3. Cells and culture

B16F10 (mouse melanoma cells), AAV293 (embryonic kidney cells) were previously stored in our laboratory. B16F10, AAV293 were cultured in Dulbecco modified Eagle medium (DMEM) (Gibco). All media contained 10% fetal bovine serum (Excel), 100 µg/mL streptomycin (Thermo Fisher) and 100 unit/mL penicillin (Thermo Fisher). All cells were cultured in incubators at 37 °C with humidification and 5% CO_2.

2.4. Preparation of phospholipids-based phase separation gel

PPSG was prepared by simple mixing. Mixed 70 mg of E80, 15 mg of soybean oil, and 12 mg of ethanol, and dissolved them thoroughly at room temperature with continuous stirring. Dissolved 1 mg anti-PD-1 polypeptide drug in 30 µL sterile water for injection, then added 30 µL anti-PD-1 solution dropwise to the PPSG, and sonicated it at a power of 70 W at 4 °C until the solution was evenly distributed in the PPSG.

2.5. Virus preparation

Recombinant AAVs were produced by triple-plasmid transduction of AAV293 cells with polyethyleneimine[30] (linear, MW 40,000; Polysciences, USA, #24765-1). Cells were harvested 72 h after transduction and suspended in TNE buffer (100 mmol/L Tris-HCl, 20 mmol/L EDTA, 150 mmol/L NaCl, pH 8.0) and subjected to 3 freeze−thaw cycles. Crude lysates containing AAV were treated with Benzonase and 10% deoxycholic acid for 1 h at 37 °C to remove residual DNA and centrifuged at $10,000 \times g$ for 30 min. Meanwhile, AAV released into the medium was recovered by addition of PEG/NaCl solution [10% polyethylene glycol 8000 (*w/v*), 0.5 mol/L NaCl] and subsequent precipitation at 4 °C for 16 h. Prior to AAV purification, AAV-containing resuspension buffer was centrifuged through an iodixanol (Sigma, USA, #D1556) gradient followed by affinity chromatography (Thermo, USA, POROS™ CaptureSelect™ AAVX Affinity Resin, #A36745) Purify.

2.6. Western blot

B16F10 cells were first seeded in a 6-well plate at a density of 2×10^5 cells per well. After 4 h, the medium was discarded and the cells were treated with 2 mL of fresh medium containing PBS, AAV-PTEN[R], or AAV-PTEN [multiplicity of infection (MOI) = 1×10^5] for 48 h and then collected in a 2-mL tube and resuspended with 200 µL of lysis buffer [50 mmol/L Tris-HCl (pH 7.4), 150 mmol/L NaCl, 1% NP-40, 0.1% SDS, and protease inhibitor]. After the protein concentration was determined by the BCA Protein Assay Kit (Beyotime Biotechnology), a sample of 100 µg protein was run through an SDS-polyacrylamide gel electrophoresis gel and then transferred to a nitrocellulose membrane blot. Next, the membrane blots were soaked in blocking buffer [5% (*w/v*) nonfat milk, TBST buffer (50 mmol/L Tris-HCl, pH 7.6 and 150 mmol/L NaCl and 0.05% Tween 20)] for 1 h. Membrane blots were then incubated overnight in appropriate dilutions of primary antibody solution at 4 °C. Membrane blots were washed 3 times with TBST buffer and incubated with horseradish peroxidase-conjugated secondary antibody at 1:5000 dilution for 1 h at 37 °C. Finally, protein signals were detected by an enhanced chemiluminescence detection system (Amersham/GE Healthcare) using a Typhoon Trio variable mode imager.

2.7. Screening of AAV serotypes

B16F10 cells were first seeded in a 12-well plate at a density of 1×10^5 cells per well. After 4 h, medium was discarded and the cells were treated with 1 mL of fresh medium containing PBS, AAV1-CAG-mCherry, AAV7m8-CAG-mCherry, AAV6-CAG-mCherry, AAV7-CAG-mCherry, AAV8-CAG-mCherry, AAV9-CAG-mCherry, AAV10-CAG-mCherry (MOI = 1×10^5) for 48 h. After 48 h, cells were first photographed by confocal microscopy and collected in 1.5-mL tubes, and resuspend with PBS for flow cytometry test.

2.8. In vitro apoptosis evaluation

Apoptosis was also detected by flow cytometry using annexin PI/AnnexinV−FITC double-staining assay. Briefly, the B16F10 cells

were seeded in 6-well plates and then treated with PBS, AAV-PTEN^R, or AAV-PTEN for 48 h. The treated B16F10 cells were first photographed by confocal microscopy and then collected, washed with PBS, and resuspended in PBS with PI and AnnexinV−FITC solution and finally were analyzed by flow cytometry.

2.9. Cell immunofluorescent staining

Cells were seeded into confocal plates at a density of 2×10^5 cells per well and incubated with 1 mL of medium containing 10% FBS for 4 h. Added 1 mL of fresh medium containing PBS, AAV-PTEN^R, or AAV-PTEN to each well. After 48 h, cells were washed with TBS buffer (50 mmol/L Tris-HCl, pH 7.6 and 150 mmol/L NaCl) and fixed with 4% paraformaldehyde for 15 min at room temperature. Next, cells were permeabilized with 0.1% Triton X-100 TBS for 10 min (this step is not required for detection of CRT) and then incubated with blocking buffer containing 5% bovine serum albumin (BSA) for 30 min at 37 °C. Then, the blocking buffer was discarded, and the cell samples were incubated with primary antibodies (such as anti-PTEN and anti-CRT) at 1:100 dilution overnight at 4 °C, washed 3 times with TBS, and incubated in secondary antibodies (1:500) with FITC or Cy3 for 30 min at 37 °C. Finally, cells were covered with anti-fluorescence quencher (Beyotime Biotechnology) containing 4′,6-diamidino-2-phenylindole (DAPI) and imaged using an Olympus CLSM (FV1000) (Zeiss, Germany).

2.10. Animal

6-week-old C57BL/6 mice were purchased from Dashuo Biotechnology (Chengdu, China). All animal experimental studies followed the requirements of the National Laboratory Animal Use Law (China). The breeding methods and environment of all experimental animals were approved by the Institutional Animal Care and Ethics Committee of Sichuan University (approval number SYXK2018-113). All animal experiments were performed under pathogen-free conditions. The experimental animals were euthanized when their body weight dropped by more than 20% continuously. The tumor volume of all tumor-receiving mice did not exceed 2000 mm^3.

2.11. Antitumor immune effects induced by AAV-PTEN

To construct a B16F10-bearing tumor mouse model, 4×10^5 B16F10 cells in 50 μL PBS were implanted subcutaneously in the right flank of 6-week-old male C57BL/6 mice. Mice were randomly divided into three groups ($n = 8$ mice per group), and on Day 7 after tumor implantation, mice were injected intratumorally with PBS, AAV-PTEN^R, and AAV-PTEN. The mice tumor volume and body weight were measured every two days thereafter.

In order to detect various immune indicators of mouse tumor tissues, the same method was used to construct a B16F10 tumor-bearing mouse model and the same dosing regimen was implemented ($n = 5$ mice per group) on Day 15 after tumor implantation. Mice were euthanized on Day 15 after tumor implantation and axillary lymph nodes and tumors were divided for the number and phenotype of each immune cell, the concentration of secreted cytokines, and the ICD index.

2.12. Therapeutic efficacy and mechanisms of triple therapy in the B16F10-bearing tumor mouse model

For in vivo therapeutic effects, a B16F10-bearing tumor mouse model was constructed as described above. B16F10 tumor-bearing mice were randomly divided into five groups ($n = 10$ mice per group): Blank group, PPSG$^{@anti-PD-1}$+CpG group, PTEN group, PTEN+PPSG$^{@anti-PD-1}$ group, and triple therapy group. On Day 7 after tumor implantation, mice in groups were injected intratumorally with PBS or AAV-PTEN (1.5×10^{10} v.g. in 5 μL PBS per mouse), and PPSG$^{@anti-PD-1}$ (100 μg anti-PD-1 in 100 μL PPSG per mouse) was injected subcutaneously around the tumor. On Days 9 and 11 after tumor implantation, CpG (3 μg in 25 μL saline per mouse) was injected subcutaneously in the right forearm of mice. Tumor size was measured every 2 days, and tumor volume was calculated according to Eq. (1):

$$\text{Tumor volume} = {}^1\!/_2\,(\text{Length} \times \text{Width} \times \text{Width}) \tag{1}$$

For mechanisms, the same tumor model construction protocol as well as treatment protocol was implemented as described above ($n = 4$ mice per group). On Day 18, the mice were euthanized. The mice were dissected, and the tumors, axillary lymph nodes and spleen were harvested for grinding, fixation, embedding, and lysis. The number and phenotype of immune cells in tumors, axillary lymph nodes, and spleen were measured. The concentration of cytokines in tumor tissues and the effect of ICD and the titer of specific antibodies in blood were also measured.

2.13. Re-challenging tumor-eradicated mice with subcutaneous B16F10 cells

On Day 90, five fresh C57BL/6 mice, two tumor-eradicated mice in the PTEN group, four tumor-eradicated mice in the PTEN+PPSG$^{@anti-PD-1}$ group, and five tumor-eradicated mice in the triple therapy group were subcutaneously injected with B16F10 cells (4×10^5 cells in 50 μL PBS per mouse) on the contralateral side of the first tumor on Day 90. Tumor volume was measured every two days when tumors could be observed.

2.14. Analysis of immune cells by flow cytometry

Tumors, axillary lymph nodes and spleen were triturated and tissue homogenates were passed through a 70 μm mesh nylon cell strainer (Biosharp) to prepare single cell suspensions. For flow cytometric analysis of surface markers, cells were stained with fluorescent-conjugated antibodies for 40 min at 4 °C. For staining of intracellular markers (e.g., TNF-α), cells were pre-stimulated with B16F10 tumor cell lysate for 6 h at 37 °C, and then stained using an intracellular factor staining kit (BD Biosciences). Fixed and permeabilized for 30 min at 4 °C. Then, intracellular marker antibodies and other surface antibodies were stained for 30 min at 4 °C. Stained cells were finally detected by flow cytometry and analyzed using FlowJo software.

2.15. HMGB1, ATP, antibody titers and cytokine detection

To examine the release of HMGB1 and ATP from B16F10 cells, B16F10 cells were first seeded in 12-well plates at a density of 1×10^5 cells/well and incubated with 1 mL of medium containing

10% FBS for 4 h. The medium was removed, and then added 1 mL of fresh medium containing PBS, AAV-PTEN^R and AAV-PTEN incubating for 48 h. Cell culture supernatants were collected and measured using ATP (Beyotime Biotechnology) and HMGB1 (Rui Xin) ELISA kits according to the kit's instructions. To assess intratumoral ATP, HMGB1, and cytokines such as IL-12p70, TNF-α, IFN-γ, tumor tissues were collected and homogenized in cold PBS buffer. The supernatant of the tumor homogenate was then assayed with an ELISA kit (cytokine kit from Invitrogen) following the kit's instructions. To measure cytokine release after splenocytes were stimulated, splenocytes were seeded in 12-well plates at a density of 1×10^7 cells/well and incubated with 1 mL of medium containing 10% FBS. B16F10 cell lysate was added to stimulate for 6 h, and the culture was continued for 72 h. Cell culture supernatants were collected and measured using an ELISA kit according to the kit's instructions.

2.16.   Immunofluorescence and H&E staining for tissues

At the end point of treatment, the mice were euthanized. The tumors and various organs (lung, heart, liver, kidney, and spleen) were harvested and fixed with 4% paraformaldehyde. All organs were embedded in paraffin and sectioned into slices at a thickness of 5 μm. The paraffin embedded sections were deparaffinized, rehydrated in a graded ethanol series, and washed in distilled water. Sample sections were then incubated in 0.3% hydrogen peroxide for 20 min to quench the activity of endogenous peroxidase, followed by antigen retrieval in citrate buffer (10 mmol/L, pH 6) for 30 min. After washing with PBS, the samples were incubated in blocking buffer (1% BSA and 5% normal goat serum) for 60 min. For immunofluorescence staining, samples were incubated with different primary rabbit antibodies (CRT and PTEN) at a 1:50 dilution overnight at 4 °C, washed with PBS, and incubated with fluorescently labeled secondary antibodies (1:1000) for 60 min at room temperature. For H&E staining, sections were stained using an assay kit (Vector Laboratories) according to the manufacturers' protocols. Last, the slides were imaged using a confocal microscope (Olympus FluoView FV1000).

3.   Results

3.1.   Screening and characterization of AAV capsids for efficient PTEN gene delivery to B16F10 cells

In order to efficiently deliver the PTEN gene into B16F10 cells, we first screened the serotype of AAV. Using mCherry as the target gene and CAG promoter highly expressed in mammalian cells, we packaged and purified seven kinds of AAV-CAG-mCherry (hereafter AAV-mCherry) with different serotypes, including AAV1-mCherry, AAV7m8-mCherry, AAV6-mCherry, AAV7-mCherry, AAV8-mCherry, AAV9-mCherry, AAV10-mCherry. Next, we investigated the infection efficiency of B16F10 by AAV-mCherry of different serotypes (Fig. 1A). B16F10 cells were treated with AAV-mCherry for 48 h at MOI, v.g. number × cell^{-1} = 1×10^5, and the expression of mCherry was confirmed by fluorescence of CLSM (Fig. 1B). Cells were then collected for flow cytometry analysis. The results showed that AAV6 could infect more than 91% of B16F10 cells at MOI = 1×10^5 (Fig. 1C), while AAV7m8 and AAV8 could infect no more than 44% of B16F10 cells. Other serotypes of AAV are less efficient at infecting B16F10 cells. Finally, we chose serotype

6 of AAV to efficiently deliver the PTEN gene. Then, we packaged and purified AAV6-CAG-PTEN (hereafter AAV-PTEN) (Fig. 1D). While we reversed the PTEN gene sequence and packaged AAV6-CAG-PTEN^R (hereafter AAV-PTEN^R) (Fig. 1D) as a vector control. We characterized them by transmission electron microscopy (Fig. 1E) and silver staining (Supporting Information Fig. S1), and the results showed that we obtained AAV6-PTEN with a high purity and low empty shell rate.

3.2.   PTEN restoration by AA6-PTEN induces apoptosis and immunogenic cell death

It has been previously reported that restoring the expression of the PTEN gene in human cancer cells could inhibit their growth[31]. Therefore, we first wanted to determine whether AAV-PTEN could efficiently restore PTEN expression in B16F10 cells *in vitro*. B16F10 cells were treated with PBS (Blank), AAV-PTEN^R (Vector), Polyethylenimine (PEI, MW 40k)-plasmid complex or AAV-PTEN (PTEN) for 48h at MOI = 1×10^5, and the expression of PTEN was confirmed by Western blot. The results showed that AAV-PTEN significantly increased the expression of PTEN in B16F10 cells (Fig. 2D). We next wanted to determine whether treatment with AAV-PTEN could inhibit the growth of B16F10 cells. B16F10 cells were treated with PBS, AAV-PTEN^R, AAV-PTEN at different MOI for 48 h, and then cell viability was measured. Even at high MOI (1×10^6), AAV-PTEN^R showed negligible toxicity to B16F10 cells (Fig. 2A). However, after treatment with AAV-PTEN, more dead cells were detected, and the IC$_{50}$ was 9.7×10^4 v.g./cell (Fig. 2A). After AAV-PTEN treatment, the morphology of B16F10 cells was examined using conventional microscopic imaging, which showed obvious apoptotic phenomena: cells shrunken and apoptotic bodies appeared around the cells (Fig. 2B). We also confirmed that AAV-PTEN treatment effectively promoted apoptosis of B16F10 cells by measuring annexin V-fluorescein isothiocyanate (FITC)/propidium iodide (PI). The apoptosis ratio of AAV-PTEN^R treatment did not increase, indicating that AAV vector did not induce apoptosis of B16F10 (Fig. 2C). However, AAV6-PTEN treatment significantly increased late apoptotic cells. The proportion of apoptotic cells after AAV6-PTEN treatment increased approximately 7-fold compared to the control group (Fig. 2C).

It has been demonstrated that activation of PTEN could promote the release of DAMPs and trigger immunogenic cell death[20]. To confirm this, three hallmark markers characterizing the effect of ICD, CRT on the cell membrane, HMGB1 and ATP released into the extracellular milieu, were measured in B16F10 cells as well as in the culture supernatant after 48 h treatment with PBS, AAV-PTEN^R or AAV-PTEN. CRT exposure on the cell membrane was confirmed by immunofluorescence with CLSM. Treatment with AAV-PTEN induced a significant increase in CRT expression on the cell membrane (Fig. 2E). The content of ATP or HMGB1 in cell culture supernatants was measured by enzyme-linked immunosorbent assay (ELISA). HMGB1 and ATP release were significantly increased in B16F10 cells treated with AAV-PTEN compared with controls (Fig. 2F and G). These results suggest that AAV6-PTEN treatment can induce apoptosis, while triggering ICD.

3.3.   AAV-PTEN induces antitumor immune responses in vivo

The ability of AAV-PTEN to induce tumor cell apoptosis and generate ICD *in vitro* inspired us to further explore whether AAV-PTEN could induce tumor cell apoptosis and activate
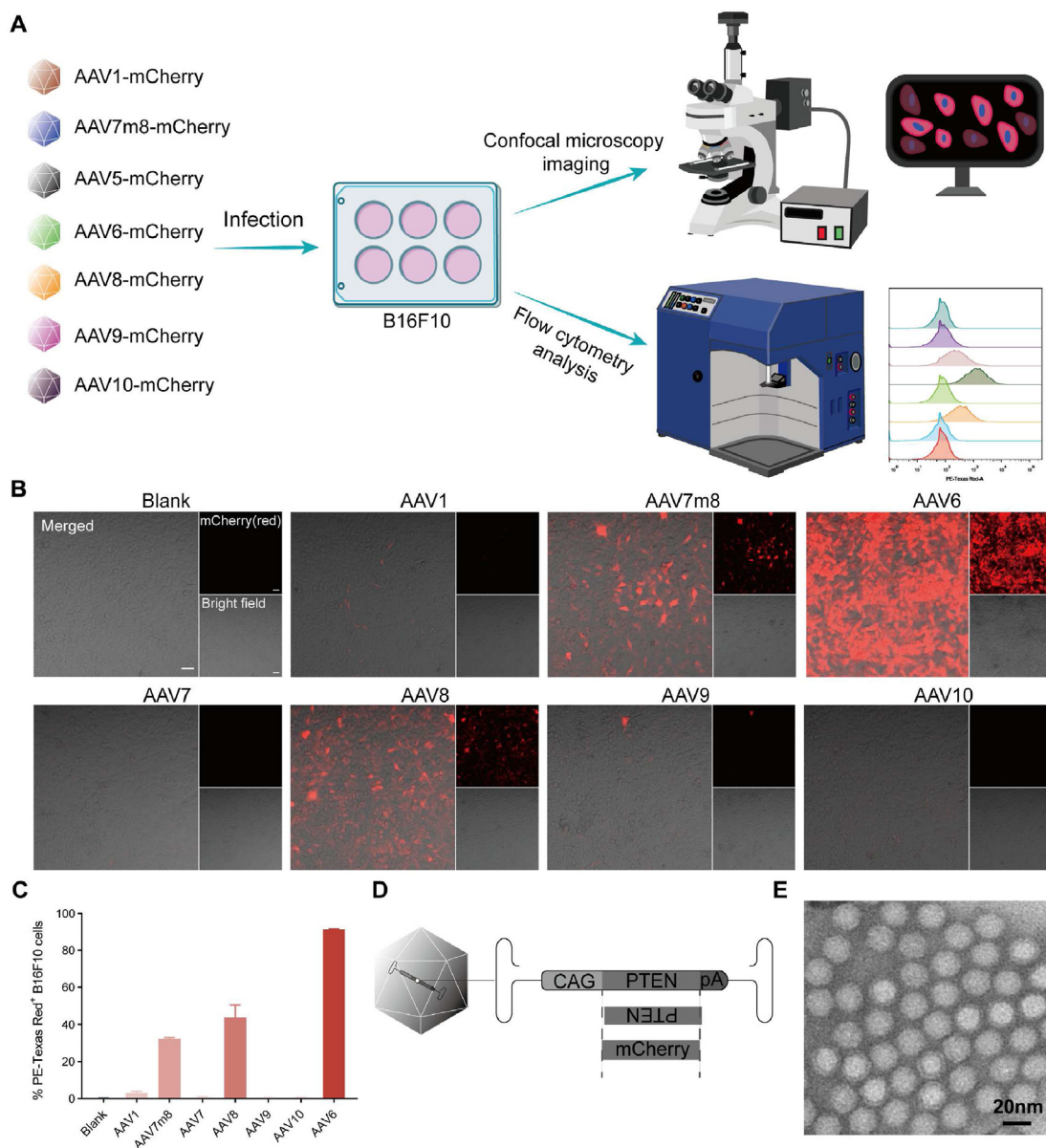
Figure 1   Screening and characterization of AAV capsids for efficient PTEN gene delivery to B16F10 cells. (A) Schematic diagram of AAV capsids screening for efficient gene delivery to B16F10 cells. (B) Confocal microscopy imaging of mCherry (red) expression in B16F10 cells treated with different serotypes of AAV-mCherry for 48 h at MOI $= 1 \times 10^5$. Scale bar, 50 μm. (C) Flow cytometry analysis of PE-Texas Red$^+$ B16F10 cells treated with different serotypes of AAV-mCherry for 48 h at MOI $= 1 \times 10^5$. Data were presented as means $\pm$ SD ($n = 3$ replicates per group). (D) Schematic of AAV-PTEN, AAV-PTEN^R and AAV-mCherry using CAG promoter highly expressed in mammalian cells. (E) TEM image of AAV6-PTEN. Scale bar, 20 nm.

anti-tumor immune responses *in vivo*. We selected C57BL/6 mice to construct a subcutaneous B16F10 tumor model and first verified whether AAV-PTEN could restore the expression of PTEN gene in B16F10 tumor-bearing mice. 96 h after intratumoral injection of PBS, AAV-PTEN^R or AAV-PTEN into B16F10 tumor-bearing mice, we confirmed the expression of PTEN in tumor tissues by immunofluorescence with CLSM. The results showed the tumor tissues of mice injected with AAV-PTEN highly expressed PTEN gene (Fig. 3D). To investigate the dose-dependence of tumor growth on AAV-PTEN, we established the B16F10 tumor-bearing mouse model. When the tumor volume reached 30 mm^3, B16F10 tumor-bearing mice were randomly assigned to five groups and

intratumorally injected with PBS (5 μL per mouse as the Blank group), AAV-PTEN^R (Vector 1.5×10^{10} v.g. in 5 μL PBS per mouse) or AAV-PTEN (L-PTEN 3×10^9 v.g., M-PTEN 1.5×10^{10} v.g., H-PTEN 7.5×10^{10} v.g. in 5 μL PBS per mouse). Mice tumor volume and body weight were measured every two days. The results demonstrated that AAV-PTEN showed a dose-dependent tumor growth inhibition, but there was no significant increase in tumor inhibition when the doses are higher than 1.5×10^{10} v.g. per mouse (Supporting Information Fig. S2).

Then, we assessed the antitumor immune response of AAV-PTEN *in vivo* using the B16F10 tumor-bearing mouse model. First, B16F10 cells were implanted subcutaneously on the right
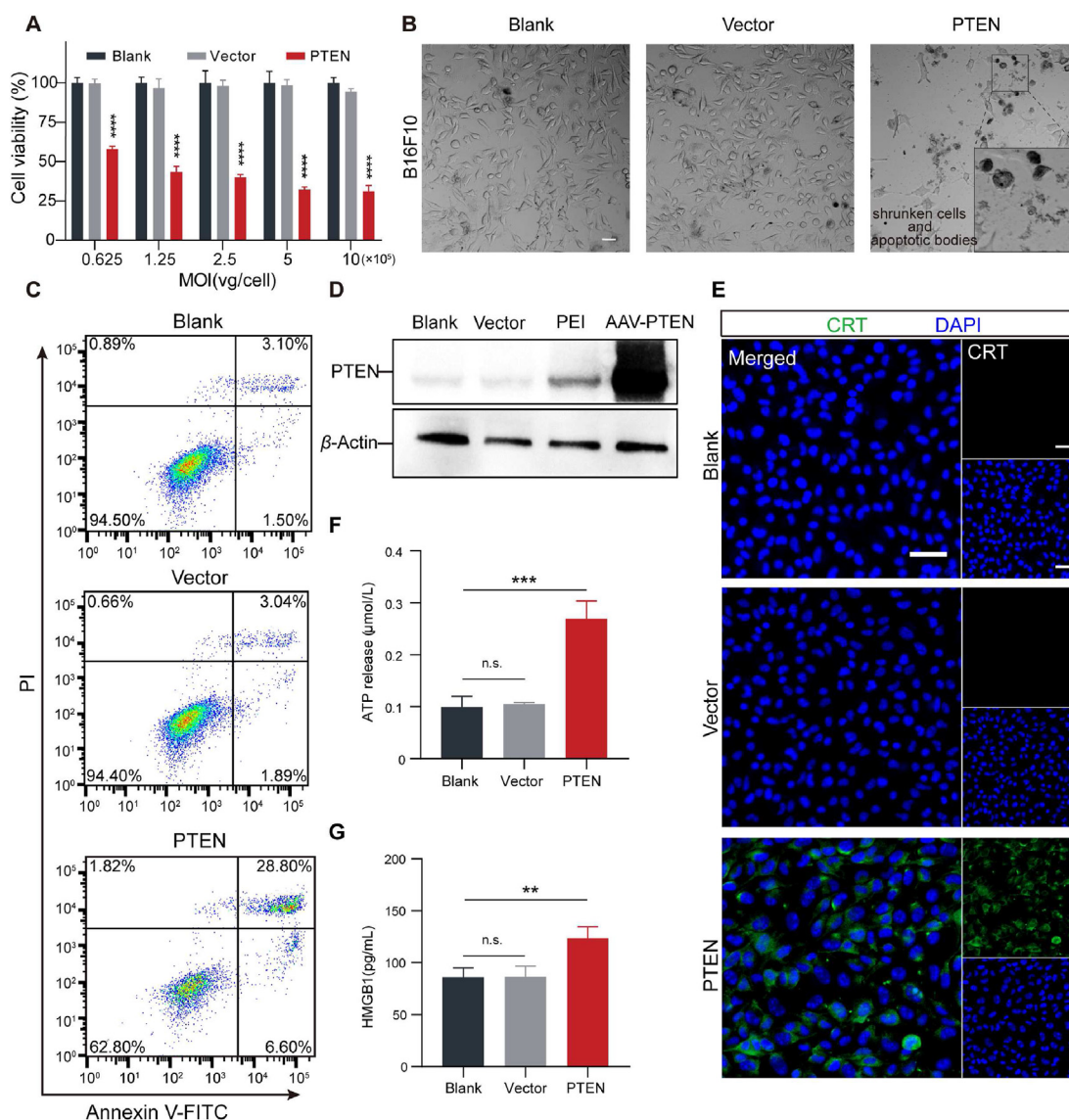
Figure 2 AA6-PTEN treatment induces apoptosis and immunogenic cell death. (A) Cell viability of B16F10 cells after treatment with AAV6-PTEN for 48 h. Data were presented as means ± SD (n = 4 replicates). Statistical significance was determined using a two-tailed Student's t test, ****P < 0.0001. (B) Conventional microscopic imaging for the morphology of B16F10 cells after indicated treatment for 48 h. (C) Apoptosis of B16F10 cells after indicated treatment for 48 h by measuring annexin V-fluorescein isothiocyanate (FITC)/propidium iodide (PI). (D) Western blot analysis of PTEN expression in B16F10 cells after the indicated treatments for 48 h. (E−G) Measurement of ICD markers in B16F10 cells after AAV6-PTEN treatment for 48 h. (E) Immunofluorescence imaging of CRT (green) expression on the B16F10 cells membrane. Scale bar, 50 μm. ATP release (F) and HMGB1 release (G) were measured by ELISA. Data were presented as means ± SD (n = 3 replicates). Statistical significance was determined using one-way ANOVA. n.s. not significant, **P < 0.01 and ***P < 0.001.

back of mice to establish B16F10 subcutaneous tumors. When the average tumor volume reached 30 mm^3, the B16F10 tumor-bearing mice were randomly divided into three groups and intra-tumorally injected with PBS (5 μL per mouse), AAV-PTEN^R (1.5 × 10^{10} v.g. in 5 μL PBS per mouse) or AAV-PTEN (1.5 × 10^{10} v.g. in 5 μL PBS per mouse). Mice tumor volume and body weight were measured every two days. Mice were euthanized on Day 15 and axillary lymph nodes and tumors were harvested to assess phenotype and number of immune cells and ICD (Fig. 3A). According to the tumor growth curve and tumor weight, AAV-PTEN showed a strong ability to inhibit tumor growth (Fig. 3B and C). Mature DCs are thought to present

antigens to T cells and are therefore important for antitumor im-mune responses. Therefore, we analyzed the maturation of tumor-draining lymph node resident DCs (LNDCs) after treatment with AAV-PTEN. The expression of various maturation markers (including CD80, CD86) on LNDCs was up-regulated after treatment (Fig. 3E). In addition, the proportions of mature DCs (CD11c$^+$ CD86$^+$) and M1-type macrophages (CD11b$^+$ F4/80$^+$ CD86$^+$) were also increased in tumors (Fig. 3F and G). On the contrary, the proportion of M2-type macrophages (CD11b$^+$ F4/80$^+$ CD206$^+$) greatly decreased (Fig. 3H). The proportions of activated CD8$^+$ effector T cells as well as activated CD4$^+$ helper T cells were up-regulated in tumors compared with control-treated
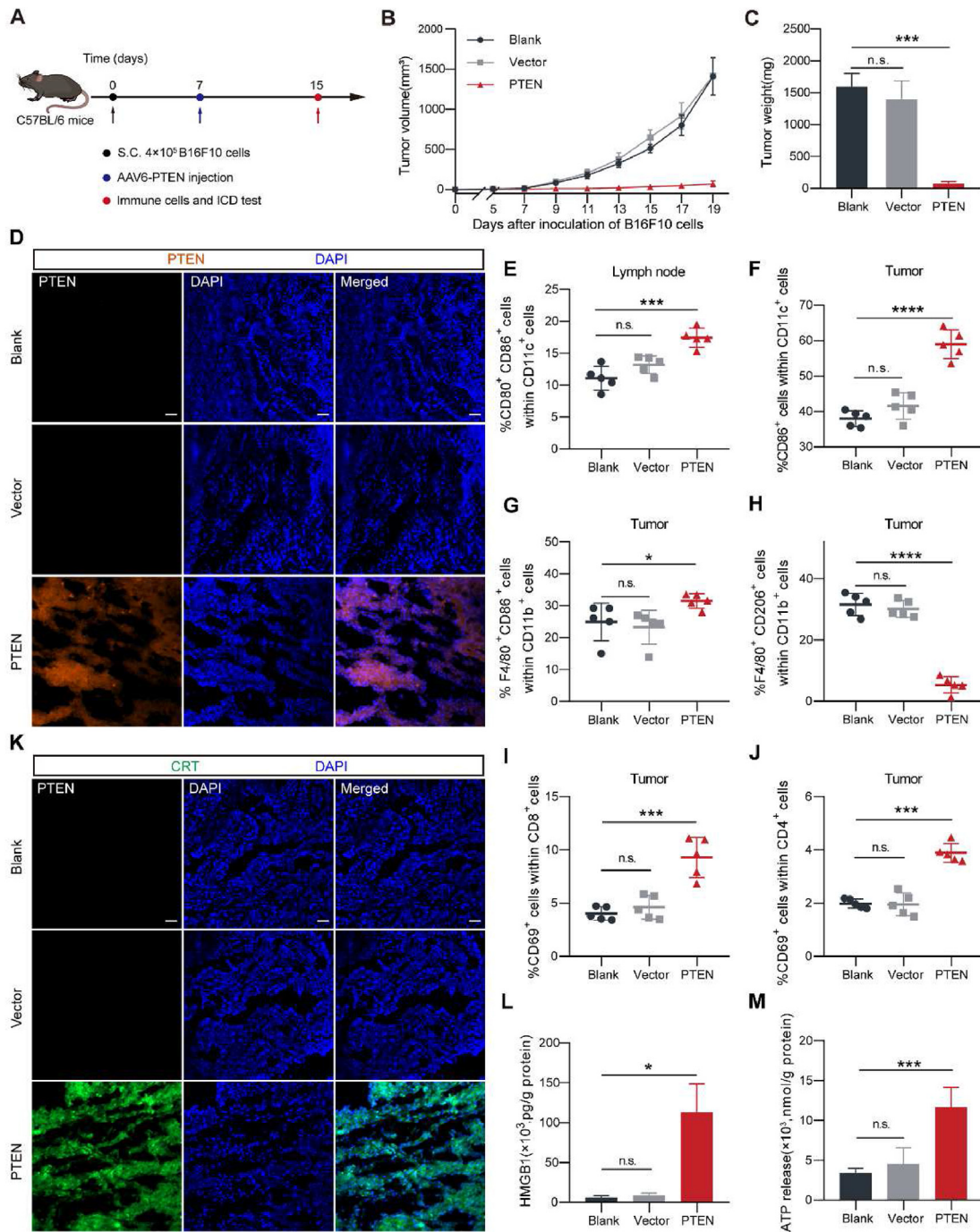
Figure 3 AAV6-PTEN induces antitumor immune responses *in vivo*. (A) Schematic illustration of the treatment of B16F10 tumor-bearing mice. S.C., subcutaneous; (B) The tumor growth curves for mice after indicated treatment. Data are displayed as means ± SEM ($n = 8$ mice per group). (C) Tumor weights in B16F10 tumor-bearing mice after seven days of treatment with AAV6-PTEN. Data are displayed as mean ± SD ($n = 8$ mice per group). (D) Immunofluorescence imaging of PTEN (red) expression in tumor tissues treated with AAV6-PTEN treatment. Scale bar, 50 μm. (E) Flow cytometry analysis of percentage of mature DCs (CD11c$^+$ CD86$^+$ CD80$^+$ cells) in TDLNs. (F–J) Flow cytometry analysis of changes in the number and phenotype of immune cells in tumor tissues. Percentage of mature DCs (CD11c$^+$ CD86$^+$ cells) (F). Percentage of M1 macrophages (CD11b$^+$ F4/80$^+$ CD86$^+$ cells) (G) and M2 macrophages (CD11b$^+$ F4/80$^+$ CD206$^+$ cells) (H). Percentage of activated CD8$^+$T cells (CD3$^+$CD8$^+$CD69$^+$ cells) (I) and activated CD4$^+$T cells (CD3$^+$CD4$^+$CD69$^+$cells) (J). (K–M) Analysis of ICD markers in mouse tumor tissues after indicated treatment. (K) Analysis of the expression of CRT in tumor tissues by immunofluorescence imaging. Scale bar, 50 μm. HMGB1 release (L) and ATP release (M) were measured by ELISA. Data were presented as means ± SD ($n = 5$ replicates). Statistical significance was determined using one-way ANOVA. n.s. not significant, $*P < 0.05$, $**P < 0.01$, $***P < 0.001$, $****P < 0.0001$.

animals (Fig. 3I and J), as assessed by flow cytometry, and the above results indicated that AAV6-PTEN treatment increased the infiltration of tumor immune cells and reversed the tumor immunosuppressive TME.

We further tested generation of the ICD *in vivo* by ELISA and immunofluorescence. We measured HMGB1 and ATP release in tumor tissues by ELISA and showed that HMGB1 and ATP release were significantly increased after mice were treated with AAV-PTEN (Fig. 3L and M). Meanwhile, immunofluorescence staining results also showed high expression of CRT from tumor tissues of mice treated with AAV-PTEN (Fig. 3K). Together, these results demonstrated that restoration of PTEN *via* AAV-PTEN effectively induced ICD *in vivo*.

3.4. Biodistribution of AAV-PTEN after intratumoral injection

For the biodistribution study of AAV-PTEN, luciferase genes were used as reporter genes and B16F10 tumor-bearing mice received an intratumoral injection of PBS or AAV- Luciferase (hereafter AAV-Luc) at a dose of 1.5×10^{10} v.g. per mouse. Three days later, major organs and tumours were collected and fully ground using a cryogenic grinder. The genomes of organs and tumors were

extracted and purified using viral DNA/RNA extraction kits (Accurate Biotechnology, China). Titers of the AAV-Luc were determined by TaqMan qPCR. The results showed that more than 95% of AAV-Luc accumulated in tumor tissue after intratumoral injection of AAV-Luc, while only a minimal amount of AAV-Luc was found in other organs (Fig. 4A).

3.5. Preparation and characterization of PPSG@anti-PD-1

In order to reduce the systemic adverse reactions of anti-PD-1 and reduce the number of administrations, we used a novel sustained-release anti-PD-1 delivery system, PPSG which had been developed for the sustained delivery of drugs in our laboratory earlier[32,33]. In this study, PPSG was prepared by simple mixing of E80 phospholipid, soybean oil and ethanol for subcutaneous delivery of anti-PD-1. The aqueous solution of anti-PD-1 was added dropwise to PPSG to obtain PPSG@anti-PD-1. There was no difference in appearance between PPSG and PPSG@anti-PD-1, showing a yellow transparent and flowable sol state (Fig. 4B). The sol state of PPSG@anti-PD-1 has a low viscosity of ≈ 630 cP, making it easier to inject subcutaneously into mice (Fig. 4C). To simulate the phase transition of PPSG@anti-PD-1 injected into mice,
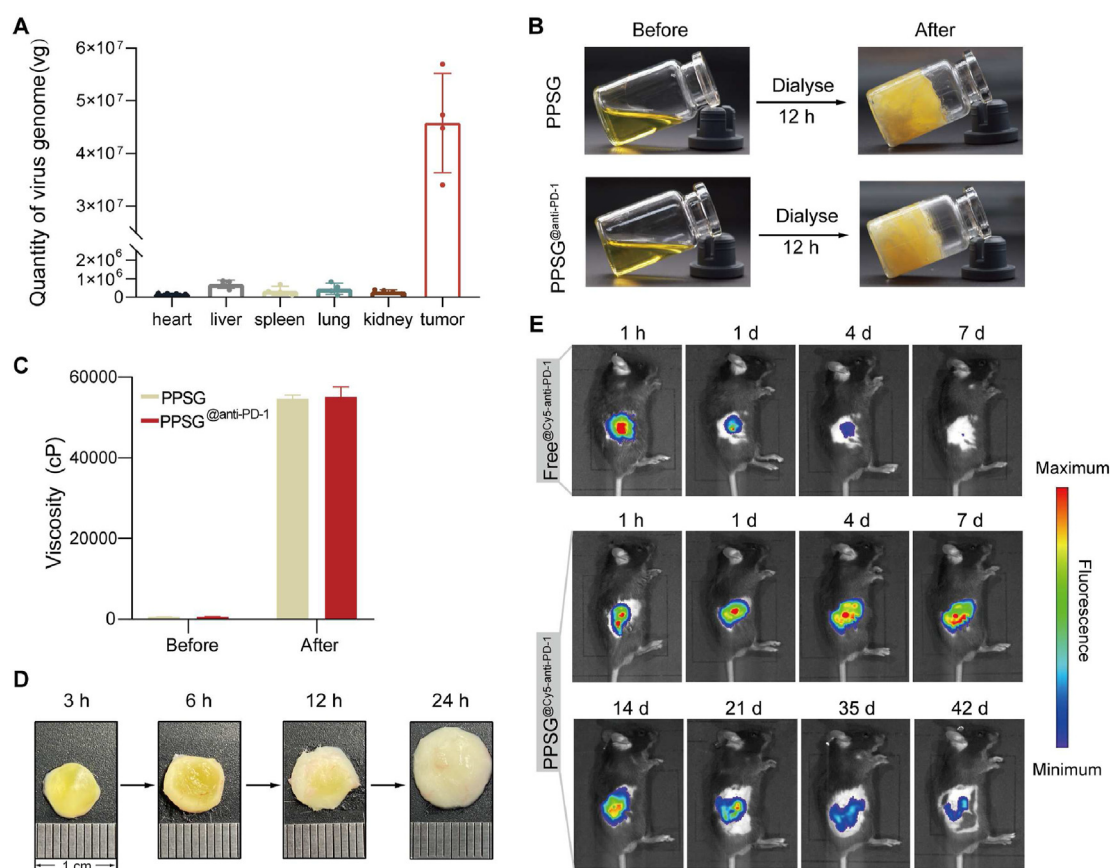
Figure 4 Biodistribution of AAV-Luciferase, characterization of PPSG and the peptide depot effect of PPSG. (A) Biodistribution of AAV-Luciferase in major organs and tumors 3 days post injection. Data are displayed as mean $\pm$ SD ($n = 4$ mice per group). (B) Appearance and fluidity of PPSG and PPSG@anti-PD-1 before and after phase transition (PPSG was dialyzed in PBS for 12 h at 37 °C) *in vitro*. (C) Viscosity of PPSG and PPSG@anti-PD-1 before and after phase transition *in vitro*. Data were presented as means $\pm$ SD ($n = 4$ replicates). (D) Phase transition of PPSG@anti-PD-1 *in vivo*. PPSG@anti-PD-1 was injected subcutaneously into the back of the mice, and PPSG@anti-PD-1 with different degrees of solidification was carefully removed from the mice after 3, 6, 12 and 24 h. (E) Peptide depot effect of PPSG@anti-PD-1 *in vivo*. Mice were injected subcutaneously with free Cy5-anti-PD-1 (Cy5-labeled anti-PD-1) or PPSG@Cy5−anti-PD-1 and imaged using the IVIS Lumina III imaging system from 1 h to 42 days post-injection.

we used a dialysis system that mimics the *in vivo* environment. PPSG@anti-PD-1 turned into a gel state with a viscosity of ≈ 55072 cP after dialysis for 12 h at 37 °C (Fig. 4B and C), then we investigated the phase transition of PPSG@anti-PD-1 in mice. PPSG@anti-PD-1 was subcutaneously injected into C57BL/6 mice, the mice were euthanized at different time points, and the gel was removed for photography. After injection, the gel gradually solidified from the outside to the inside, and the color gradually changed from yellow to white. At 6 h after injection, the exterior of PPSG solidified but the interior remained oil-like. At 24 h after injection, PPSG@anti-PD-1 turned into a semi-solid gel, which could be used as a sustainable release depot for anti-PD-1 (Fig. 4D). PPSG and PPSG@anti-PD-1 showed good stability at 4 or 37 °C, and no change in appearance was observed after 7 days (Supporting Information Fig. S3).

3.6. Sustained release of PPSG in vivo

To examine the sustained release effect of PPSG *in vivo*, we subcutaneously injected free Cy5-anti-PD-1 (Cy5-labeled anti-PD-1) or PPSG@Cy5−anti-PD-1 into C57BL/mice. Mice were then imaged *in vivo* at various time points from 1 h to 42 days after injection to observe the release of Cy5-anti-PD-1 from PPSG. We observed that in mice injected with free Cy5-anti-PD-1, the fluorescence decayed very rapidly, and the fluorescence almost disappeared by the seventh day. Compared with the free

group, the fluorescence decayed slowly in mice injected with PPSG@Cy5−anti-PD-1 and was still detectable at Day 42 (Fig. 4E). The above results show that PPSG@Cy5−anti-PD-1 has a good sustained-release effect, which can continuously release anti-PD-1 by forming a drug depot in mice subcutaneously. The excellent sustained-release effect of PPSG can greatly reduce the frequency of doses and improve patient compliance with our treatment plan on the premise of ensuring the efficacy of the drug.

3.7. Triple therapy (AAV-PTEN+PPSG@anti-PD-1+CpG) enhances antitumor effect and induces immune memory in a subcutaneous B16F10-bearing mouse model

B16F10 tumor-bearing mice were obtained by subcutaneously inoculating 4×10^5 B16F10 cells on the right back of C57BL/6 mice. B16F10 tumor-bearing mice were randomly divided into 5 groups ($n = 10$ per group): Blank group, PPSG@anti-PD-1+CpG group, PTEN group, PTEN+PPSG@anti-PD-1 group and PTEN+PPSG@anti-PD-1+CpG (hereafter triple therapy) group (Fig. 5A). On Day 7 after tumor implantation, mice in each group were injected intratumorally with PBS or AAV-PTEN (1.5×10^{10} v.g. in 5 μL PBS per mouse) and PPSG@anti-PD-1 (100 μg anti-PD-1 in 100 μL PPSG per mouse) injected subcutaneously around the tumor. On Days 9 and Day 11, CpG (3 μg in 25 μL saline per mouse) was injected subcutaneously into the right forearm of mice. After treatment, tumor volume and body weight were
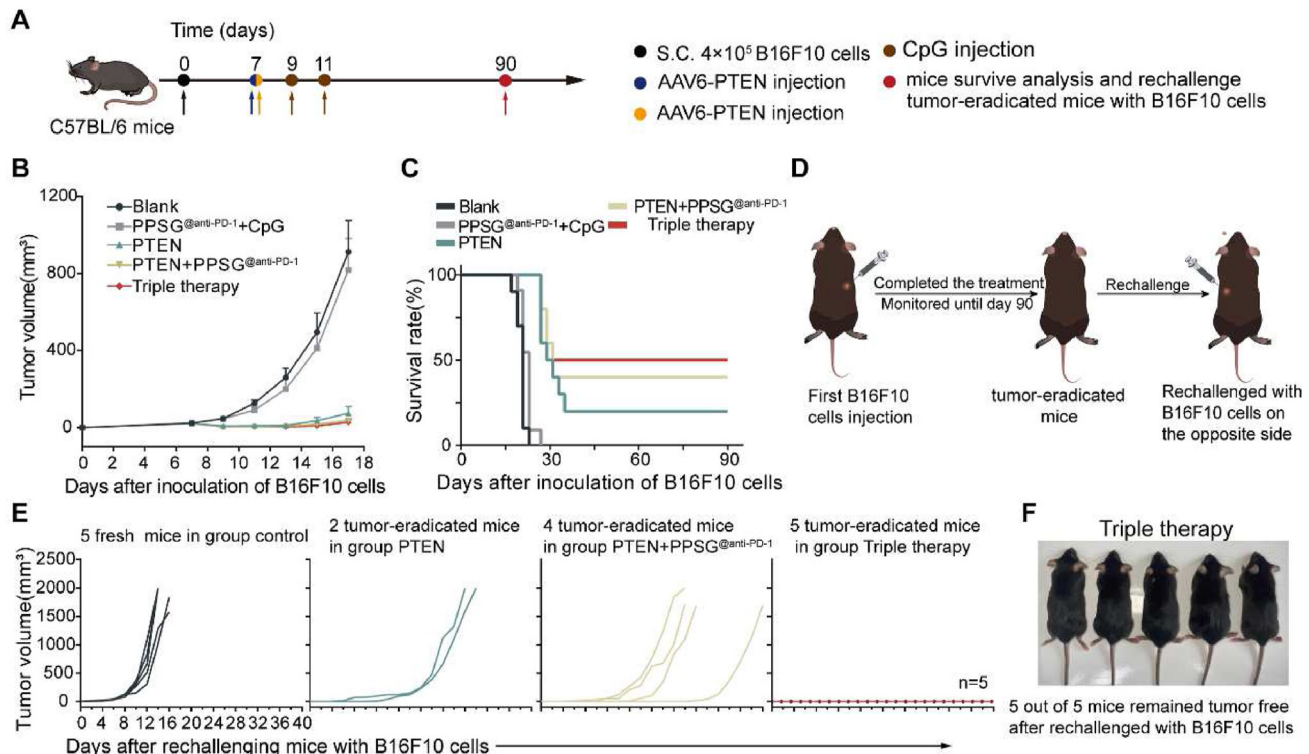
Figure 5 Synergistic therapeutic effect of the triple therapy in a subcutaneous B16F10-bearing mouse model. (A) Schematic illustration of the triple therapy treatment in B16F10 tumor-bearing mice. (B) The tumor growth curves for mice after indicated treatment. (C) Kaplan−Meier survival curves of mice treated as indicated (10 mice per group). (D) Schematic illustration of re-challenging tumor-eliminated mice with B16F10 cells. (E) Individual tumor volume growth curves for mice after re-challenged with B16F10 cells. Tumor-eradicated mice after indicated treatment (two tumor-eradicated mice in the PTEN group, four tumor-eradicated mice in the PTEN+PPSG@anti-PD-1 group, and five tumor-eradicated mice in the triple therapy group were re-challenged by subcutaneous injection of 4×10^5 B16F10 cells on the left back of the mouse. (F) Surviving mice in triple therapy group after re-challenged with B16F10 cells.
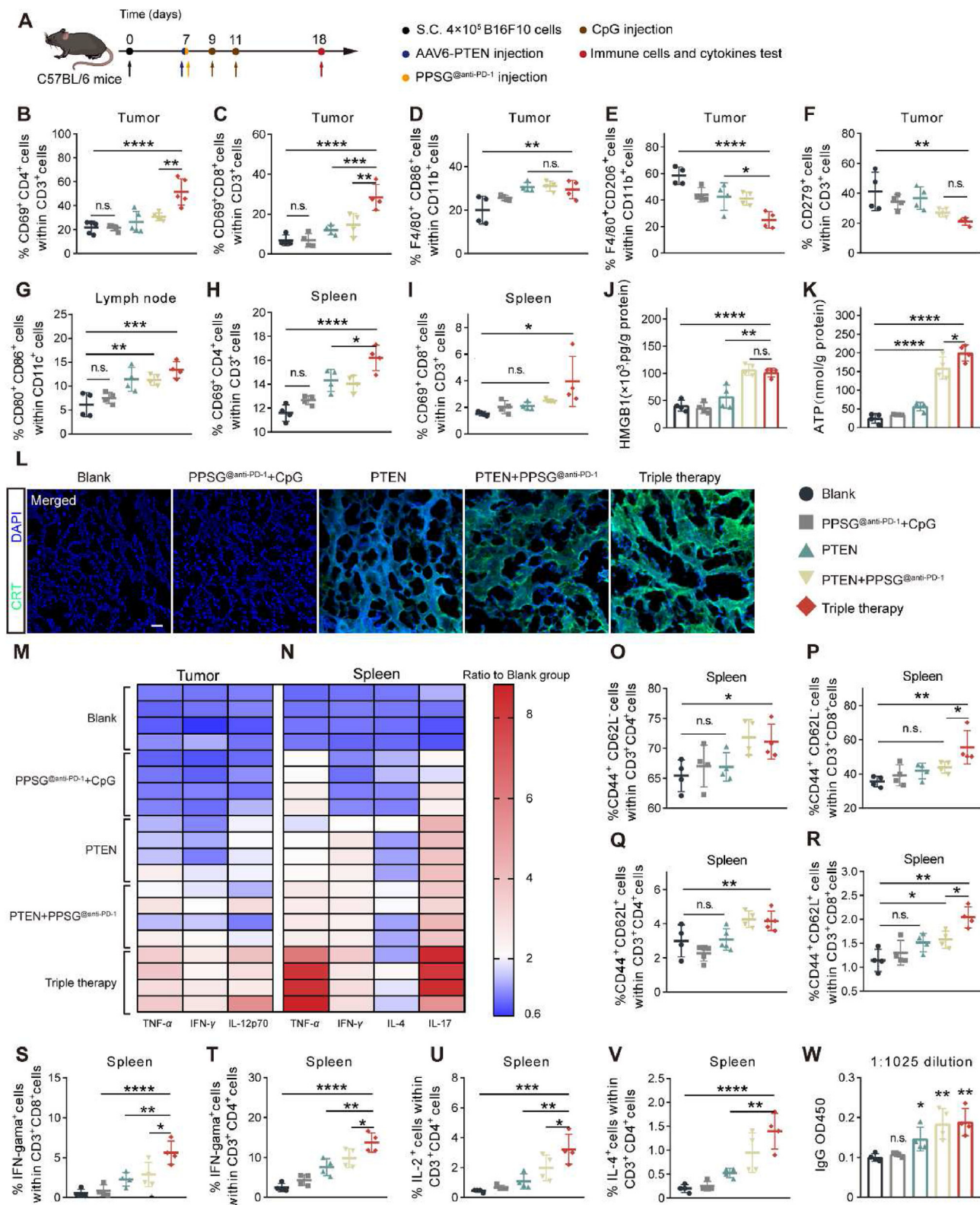
Figure 6 Immune responses and immune memory induced by triple therapy in a subcutaneous B16F10-bearing mouse model (A) Schematic illustration of triple therapy treatment in B16F10 tumor-bearing mice. (B−F) Flow cytometry analysis of changes in the number and phenotype of immune cells in tumor tissues. Percentage of activated CD4$^+$T cells (CD3$^+$CD4$^+$CD69$^+$ cells) (B) and activated CD8$^+$T cells (CD3$^+$CD8$^+$CD69$^+$ cells) (C). Percentage of M1 macrophages (CD11b$^+$ F4/80$^+$ CD86$^+$ cells) (D) and M2 macrophages (CD11b$^+$ F4/80$^+$ CD206$^+$ cells) (E). Percentage of PD-1$^+$ T cells (CD3$^+$CD279$^+$ cells) (F). (G) Flow cytometry analysis of percentage of mature DCs (CD11c$^+$ CD86$^+$ CD80$^+$ cells) in TDLNs. (H) Flow cytometry analysis of percentage of activated CD4$^+$T cells (CD3$^+$CD4$^+$CD69$^+$ cells) and (I) activated CD8$^+$T cells (CD3$^+$CD8$^+$CD69$^+$ cells) in splenocytes. (J−L) Analysis of ICD markers in mouse tumor tissues after indicated treatment. HMGB1

measured every two days, and mouse survival was monitored once a day. Compared with the blank group, the combination of PPSG$^{@anti-PD-1}$ and CpG had a weak inhibitory effect on tumors, which may be related to the resistance of PTEN-deficient B16F10 cells to ICB treatment and the inability to produce ICD to release antigens. On Day 14, 50% of the mice in the three AAV6-PTEN-treated groups remained tumor-free. Afterwards, some mice in the PTEN group and PTEN+PPSG$^{@anti-PD-1}$ group started to have tumor recurrence, but none of the tumor-eliminated mice in the triple therapy group had tumor recurrence (Fig. 5B and Supporting Information Fig. S4). PTEN treatment alone effectively inhibited tumor growth and eradicated tumors in two of ten mice. Compared with the PTEN group, the combination of PTEN and PPSG$^{@anti-PD-1}$ further inhibited tumor growth and improved the survival rate of tumor-bearing mice. PTEN and PPSG$^{@anti-PD-1}$ eradicated four out of ten mice only in the tumor. The triple therapy achieved the highest mouse survival rates, eradicating tumors in five of ten mice (Fig. 5B and C).

To explore whether the triple therapy can induce immune memory against melanoma in B16F10 tumor-bearing mice. On Day 90, tumor-eradicated mice (two tumor-eradicated mice in the PTEN group, four tumor-eradicated mice in the PTEN+PPSG$^{@anti-PD-1}$ group, and five tumor-eradicated mice in the triple therapy group) were re-challenged by subcutaneous injection of 4×10^5 B16F10 cells on the left back of the mouse (Fig. 5D). As a comparison, five 6-week-old fresh C57BL/6 in the Control group were also subcutaneously implanted with the same number of B16F10 cells on Day 0. Tumor volume and body weight were measured every two days. The tumors of the mice in the Blank group grew rapidly and all died on Day 16 (Fig. 5E). Mice in group PTEN and group PTEN+PPSG$^{@anti-PD-1}$ had delayed tumor recurrence and slow growth, but eventually all of the mice died (Fig. 5E). The tumor-eliminated mice in the triple therapy group exhibited complete rejection of the re-challenged B16F10 cells and 5 out of 5 mice remained tumor free after rechallenged with B16F10 cells (Fig. 5E). The surviving mice were monitored for an additional 5 months, and the mice had no tumor recurrence (Fig. 5F).

3.8. Mechanisms of the triple therapy to induce antitumor immune responses and prevent tumor recurrence

The above results indicated that the triple therapy achieved the best anti-tumor effect, improved the survival rate of B16F10 tumor-bearing mice and inhibited tumor recurrence. To further explore the mechanism of the triple therapy-induced antitumor immune response, we implanted 4×10^5 B16F10 cells subcutaneously on the right back of C57BL/6 mice to establish B16F10 subcutaneous tumors. Mice were treated on Days 7, 9 and 11 as described above (Fig. 6A). On Day 18, the mice were euthanized, and we analyzed the number and phenotype of immune cells in tumor tissues, axillary lymph nodes, and spleen of treated mice by flow cytometry. At the same time, we measured the specific

antibody against tumor antigen in serum, cytokines and ICD in tumor tissues by ELISA and CLSM.

First, we measured three markers of ICD in tumor tissues. Compared with the PTEN group, the ATP and HMGB1 release of the tumor tissues in the combined treatment group increased (Fig. 6J and K), and the results of immunofluorescence also showed that the expression of CRT increased after combined treatment (Fig. 6L). Based on the above results, we speculate that the enhanced effect of ICD in the combined treatment group may induce stronger anti-tumor immune responses. We examined immune cells in tumor tissues. The results showed that the triple therapy increased the infiltration of activated helper T cells (CD3$^+$ CD4$^+$ CD69$^+$) as well as effector T cells (CD3$^+$ CD8$^+$ CD69$^+$) in tumor tissues compared with the PTEN group (Fig. 6B and C). Compared with the control group, the triple therapy resulted in an increase in the proportion of M1-type macrophages (CD11b$^+$F4/80$^+$CD86$^+$) and a decrease in the proportion of M2-type macrophages (CD11b$^+$F4/80$^+$CD206$^+$) (Fig. 6D and E). We next examined the levels of tumor necrosis factor-α (TNF-α), interferon-γ (IFN-γ), and interleukin-12 (IL-12), which play important roles in cellular immunity and host defense, mainly regulating Th1 cell-mediated immune response. Compared with PTEN monotherapy, PTEN combined with PPSG$^{@anti-PD-1}$ increased the levels of TNF-α and IFN-γ in tumor tissues. Triple therapy induced the highest levels of TNF-α, IFN-γ and IL-12 (Fig. 6M). At the same time, we also detected the expression of PD-1 on the surface of T cells in tumor tissues. The results showed that the expression of PD-1 on the surface of T cells (CD3$^+$CD279$^+$) in tumor tissues was reduced in mice treated with PTEN and PPSG$^{@anti-PD-1}$ (Fig. 6F). The above results indicated that the combination of AAV-PTEN and PPSG$^{@anti-PD-1}$ better reversed the immunosuppressive TME, and the triple therapy group induced stronger antitumor immune responses.

To explore the mechanism of the triple therapy inhibiting tumor recurrence, we tested specific antibodies in the spleen, tumor-draining lymph nodes, and blood. We speculate that the triple therapy elicits an immune memory in mice that allows complete rejection of re-challenged tumor cells. Mature DCs are capable of antigen presentation, which is important for the generation of immune memory[34]. Therefore, we analyzed the maturation of tumor-draining lymph node-resident DCs (LNDCs) after treatment. Compared with PTEN monotherapy, the triple therapy induced an increase in the proportion of mature DCs (Fig. 6G). Because the specific antibodies against tumor cells in the serum can achieve anti-tumor effect by activating the complement pathway. Therefore, we also measured the titers of specific antibodies against tumor antigens in the blood of mice after treatment by Elisa. The results showed that the triple therapy had the highest antibody titers (Fig. 6W and Supporting Information Fig. S5). The spleen is the largest immune organ. A small fraction of activated T cells in the spleen can differentiate into memory T cells. When

---

release (J) and ATP release (K) were measured by ELISA. (L) Analysis of the expression of CRT in tumor tissues by immunofluorescence imaging. Scale bar, 50 μm. (M) ELISA analysis of cytokines in mice tumors ($n = 4$ mice per group), including IFN-γ, TNF-α, and IL-12p70. (N) ELISA analysis of cytokines released by splenocytes into culture supernatant, including IFN-γ, TNF-α, IL-4, IL-17. (O−R) Flow cytometry analysis of the percentages of memory T cells in splenocytes, including central memory T cells (CD44$^+$CD62L$^+$ T cells) (O, R), effector memory T cells (CD44$^+$CD62L$^-$ T cells) (P, Q). (S−V) Flow cytometry analysis of cytokine production within T cells, including IFN-γ in CD8$^+$ T cells (S), IFN-γ in CD4$^+$ T cells (T), IL-2 in CD4$^+$ T cells (U), IL-4 in CD4$^+$ T cells (V). (W) ELISA analysis of levels of antibody against B16F10 cell antigens in serum, including IgG. Data were presented as means ± SD ($n = 4$ replicates). Statistical significance was determined using one-way ANOVA. n.s. not significant, $*P < 0.05$, $**P < 0.01$, $***P < 0.001$, $****P < 0.0001$.

the immune system is exposed to the same antigen again, the memory T cells are rapidly converted into large numbers of effector T cells. Memory T cells are important for preventing tumor recurrence and achieving long-lasting protection. We measured the proportion of effector T cells, helper T cells and memory T cells in the spleen of mice after treatment. The results showed that the triple therapy increased the percentage of effector T cells as well as helper T cells (Fig. 6H and I). In addition, the triple therapy induced the highest percentages of effector memory T cells (CD44$^+$CD62L$^-$ T cells) and central memory T cells (CD44$^+$CD62L$^+$ T cells) in mouse splenocytes (Fig. 6O−R). We also detected the secretion of TNF-α and IFN-γ in splenocytes stimulated by B16F10 cell lysate. The results showed that the levels of TNF-α and IFN-γ secreted by splenocytes in the triple therapy group were the highest (Fig. 6N). We also measured cytokine production within T cells by flow cytometry. The results revealed that the proportion of effector T cells (CD8$^+$IFN-γ^+) and Th1 cells (CD4$^+$IL2$^+$, CD4$^+$IFN-γ^+) in splenocytes after triple therapy were the highest, indicating that the triple therapy induced the strongest antitumor cellular immune response (Fig. 6S−U). In addition, the proportion of Th2 cells (CD4$^+$IL-4$^+$) also showed the highest in the triple therapy group, indicating that the triple therapy can also induce specific humoral immune responses against antigens of B16F10 cells (Fig. 6V). In conclusion, the triple therapy achieves immune memory by inducing a systemic immune response against melanoma in mice, including increased memory T cells in the spleen, secretion of specific antibodies in serum, and maturation of lymph node DCs, thereby inhibiting tumor recurrence.

3.9. Safety profile of the triple therapy in vivo

To evaluate the in vivo toxicities of the triple therapy, various organs and blood of mice were collected on Day 7 after the last injection (Day 18). Organs were sectioned and stained with hematoxylin and eosin (H&E). The results showed that there was no significant difference in the tissues of the heart, liver, lung and kidney between the blank group and each treatment group, indicating that the triple therapy had no obvious toxicity to each organ of the mice (Supporting Information Fig. S6). For the hematological analysis, we tested blood routine and blood biochemical parameters. The blood routine results showed that after the triple therapy, there were no significant changes in red blood cells, white blood cells, platelets, granulocytes, monocytes, and lymphocytes in the blood of mice (Supporting Information Fig. S7). At the same time, the results of blood biochemistry showed that parameters such as Aspartate aminotransferase, alanine aminotransferase, total protein 2, uric acid 2 did not change significantly (Supporting Information Fig. S8). In addition, the triple therapy did not cause weight loss in mice (Supporting Information Fig. S9). The above results together indicate that our proposed triple therapy does not produce side effects in vivo.

4. Discussion

ICB therapy has gradually become one of the first-line therapies for cancer treatment[35]. However, due to tumor immunosuppression TME, ICB therapy alone often has relatively poor antitumor effect due to the poor responsive rate on many cancers including melanoma[7,8]. As a result, ICB therapy is usually combined with traditional therapy[1] to treat tumors, such as radiotherapy[3] and

chemotherapy[2]. However, these traditional remedies have serious side effects, including damage to tissues, low blood counts and hair loss[36]. In the current study, we innovatively combined AAV-delivered PTEN gene therapy with ICB therapy and in situ tumor vaccine therapy. Our triple therapy has shown a prominent synergistic anti-tumor effect. First, we showed that AAV-delivered PTEN gene therapy induced apoptosis of tumor cells without substantial toxicity. Meanwhile, the reversed immuno-suppressed TME by AAV-delivered PTEN gene therapy in turn enhanced the immunomodulatory effect of ICB therapy. In addition, AAV-delivered PTEN gene therapy caused tumor cells to produce ICD and release multiple tumor antigens. The released tumor antigens were combined with the strong adjuvanticity of CpG, in the form of in situ tumor vaccine, to induce DC maturation and cross-presentation to T cells. At the same time, ICB therapy blocked the suppressive effect of the tumor on T cells, thereby increasing the percentage of activated T cells. The combination therapy finally effectively inhibited tumor progression and recurrence. Our results revealed the strong clinical translation potential of this novel triple therapy for cancer immune therapy.

Previous studies have shown that the deletion of tumor suppressor gene PTEN leads to drug resistance to ICB therapy[11,37]. As a negative regulator of PI3K/AKT signaling, PTEN plays an important role in suppressing tumor growth. Therefore, PI3K inhibitors were developed to treat tumors[38]. However, PI3K inhibitors cause severe side effects and they cannot fully restore the function of the PTEN gene[39]. Therefore, it is crucial to safely and efficiently deliver PTEN gene to tumor cells in vivo. PTEN-delivery for the treatment of melanoma and use of AAV as a vector for gene delivery to melanoma remains underreported. In this work, we innovatively selected AAV as a vector to deliver PTEN gene for the treatment of melanoma and we screened AAV serotype 6 that can efficiently transduce B16F10 through in vitro infection experiments (AAV6 can efficiently transduce 91% of B16F10 cells). We further investigated the ability of AAV-PTEN to infect tumor cells in vivo. Although non cancer cells are also an important component of the cancer ecosystem, current research shows that the proportion of cancer cells exceeds 80% in melanoma[40]. Our results showed that AAV-PTEN could efficiently restore the expression of PTEN gene in tumor tissues of B16F10 tumor bearing mice. Moreover, AAV-based PTEN gene delivery requires only a single dose to achieve efficient tumor transduction, whereas a non-viral vector-based PTEN gene delivery requires more than three doses[31]. Our results suggest that AAV-based restoration of the PTEN gene in tumor cells exerts excellent anti-tumor immunity by causing tumor cell apoptosis and inducing tumor cell ICD.

It is well known that ICB therapy requires multiple doses of long-term systemic administration, which leads to poor patient compliance and may lead to systemic adverse reactions[9]. In this work, our developed PPSG$^{@anti\text{-}PD\text{-}1}$ can form an in situ depot in mice that can sustainably release anti-PD-1 drugs within 42 days. Thus, a single dose can play a long-term role in regulating the TME. Because PPSG$^{@anti\text{-}PD\text{-}1}$ is injected around the tumor, it also reduced systemic adverse reactions. Our results demonstrate that AAV-based restoration of the PTEN gene in tumor cells reverses the tumor immunosuppressive TME and improves melanoma responsiveness to ICB therapy.

Melanoma is a very complex and highly malignant solid tumor, and the recurrence of melanoma is the root cause of cancer failure in many patients[41−43]. In order to effectively inhibit the recurrence

of melanoma, we have successfully developed the triple therapy for melanoma. We introduced CpG on the basis of AAV6-PTEN combined with ICB treatment. CpG is a TLR9 agonist with potent immunostimulatory adjuvant activity and induction of Th1-type immune responses. The combination of immune adjuvants CpG and the released tumor antigens induced by the restoration of the PTEN efficiently activated the immune system. In the current study, 50% of the mice in the triple therapy group had complete tumor elimination and exhibited complete rejection of the re-challenged B16F10 cells. Although the combination of PTEN and PPSG$^{@anti-PD-1}$ could well suppress the first tumor, it could not induce immune memory and failed to suppress tumor recurrence. In comparison, the triple therapy exerted a powerful anti-tumor immune effect and effectively inhibited melanoma recurrence. Our results showed that the triple therapy induced tumor antigen-specific cellular and humoral immunity and formed long-term immune memory response.

5. Conclusions

In conclusion, we have developed a combination therapy strategy that elicits powerful and potent antitumor immune effects. Our results show that AAV-based PTEN gene delivery combined with ICB sustained-release therapy and *in situ* tumor vaccine therapy achieved synergistic anti-tumor immune effects. This triple therapy has great potential in eradicating malignant tumors and inhibiting tumor recurrence. We anticipate that this triple therapy could be developed for tumor-specific precision immunotherapy.

Acknowledgments

Author contributions

Yongshun Zhang and Xun Sun designed research; Yongshun Zhang, Lan Yang, Yangsen Ou, Rui Hu, Guangsheng Du, Shuang Luo, Fuhua Wu, Hairui Wang, Zhiqiang Xie, Yu Zhang, Chuting He and Cheng Ma performed research; Tao Gong, Ling Zhang, Zhirong Zhang and Xun Sun contributed new reagents/analytic tools; Yongshun Zhang analyzed data; and Yongshun Zhang wrote the paper.

Conflicts of interest

The authors have no conflicts of interest to declare.

Appendix A. Supporting information

Supporting data to this article can be found online at https://doi.org/10.1016/j.apsb.2023.06.006.

References

1. Gotwals P, et al. Prospects for combining targeted and conventional cancer therapy with immunotherapy. *Nat Rev Cancer* 2017;**17**: 286−301.
2. Cook AM, Lesterhuis WJ, Nowak AK, Lake RA. Chemotherapy and immunotherapy: mapping the road ahead. *Curr Opin Immunol* 2016; **39**:23−9.
3. Kuai R, et al. Elimination of established tumors with nanodisc-based combination chemoimmunotherapy. *Sci Adv* 2018;**4**:eaao1736.
4. Sharabi AB, Lim M, DeWeese TL, Drake CG. Radiation and checkpoint blockade immunotherapy: radiosensitisation and potential mechanisms of synergy. *Lancet Oncol* 2015;**16**: e498−509.
5. Ribas A, Wolchok JD. Cancer immunotherapy using checkpoint blockade. *Science* 2018;**359**:1350−5.
6. Park YJ, Kuen DS, Chung Y. Future prospects of immune checkpoint blockade in cancer: from response prediction to overcoming resistance. *Exp Mol Med* 2018;**50**:1−13.
7. Jenkins RW, Barbie DA, Flaherty KT. Mechanisms of resistance to immune checkpoint inhibitors. *Br J Cancer* 2018;**118**:9−16.
8. Binnewies M, et al. Understanding the tumor immune microenvironment (TIME) for effective therapy. *Nat Med* 2018;**24**:541−50.
9. Ramos-Casals M, et al. Immune-related adverse events of checkpoint inhibitors. *Nat Rev Dis Prim* 2020;**6**:38.
10. Milella M, et al. PTEN: multiple functions in human malignant tumors. *Front Oncol* 2015;**5**:24.
11. Peng W, et al. Loss of PTEN promotes resistance to T cell-mediated immunotherapy. *Cancer Discov* 2016;**6**:202−16.
12. George S, et al. Loss of PTEN is associated with resistance to anti-PD-1 checkpoint blockade therapy in metastatic uterine leiomyosarcoma. *Immunity* 2017;**46**:197−204.
13. Barroso-Sousa R, et al. Tumor mutational burden and PTEN alterations as molecular correlates of response to PD-1/L1 blockade in metastatic triple-negative breast cancer. *Clin Cancer Res* 2020;**26**:2565−72.
14. Roh W, et al. Integrated molecular analysis of tumor biopsies on sequential CTLA-4 and PD-1 blockade reveals markers of response and resistance. *Sci Transl Med* 2017;**9**:eaah3560.
15. Arico S, et al. The tumor suppressor PTEN positively regulates macroautophagy by inhibiting the phosphatidylinositol 3-kinase/protein kinase B pathway. *J Biol Chem* 2001; **276**:35243−6.
16. Gozuacik D, Kimchi A. Autophagy as a cell death and tumor suppressor mechanism. *Oncogene* 2004;**23**:2891−906.
17. Wang Y, Martins I, Ma Y, Kepp O, Galluzzi L, Kroemer G. Autophagy-dependent ATP release from dying cells *via* lysosomal exocytosis. *Autophagy* 2013;**9**:1624−5.
18. Michaud M, et al. Autophagy-dependent anticancer immune responses induced by chemotherapeutic agents in mice. *Science* 2011;**334**: 1573−7.
19. Ma Y, Galluzzi L, Zitvogel L, Kroemer G. Autophagy and cellular immune responses. *Immunity* 2013;**39**:211−27.
20. Krysko DV, Garg AD, Kaczmarek A, Krysko O, Agostinis P, Vandenabeele P. Immunogenic cell death and DAMPs in cancer therapy. *Nat Rev Cancer* 2012;**12**:860−75.
21. Su H, et al. Therapeutic antitumor efficacy of tumor-derived autophagosome (DRibble) vaccine on head and neck cancer. *Int J Nanomed* 2015;**10**:1921−30.
22. Viry E, et al. Autophagy: an adaptive metabolic response to stress shaping the antitumor immunity. *Biochem Pharmacol* 2014;**92**: 31−42.
23. Chaudhary N, Weissman D, Whitehead KA. mRNA vaccines for infectious diseases: principles, delivery and clinical translation. *Nat Rev Drug Discov* 2021;**20**:817−38.
24. Qin S, et al. A novel heterologous receptor-binding domain dodecamer universal mRNA vaccine against SARS-CoV-2 variants. *Acta Pharm Sin B* 2023;**13**:4291−304.

25. Wang Y, Zhang Z, Luo J, Han X, Wei Y, Wei X. mRNA vaccine: a potential therapeutic strategy. *Mol Cancer* 2021;**20**:33.
26. Li C, Samulski RJ. Engineering adeno-associated virus vectors for gene therapy. *Nat Rev Genet* 2020;**21**:255−72.
27. Enger PO, Thorsen F, Lonning PE, Bjerkvig R, Hoover F. Adeno-associated viral vectors penetrate human solid tumor tissue *in vivo* more effectively than adenoviral vectors. *Hum Gene Ther* 2002;**13**:1115−25.
28. Peng M, et al. Neoantigen vaccine: an emerging tumor immunotherapy. *Mol Cancer* 2019;**18**:128.
29. Krieg AM. CpG motifs in bacterial DNA and their immune effects. *Annu Rev Immunol* 2002;**20**:709−60.
30. Wu F, et al. Single-shot AAV-vectored vaccine against SARS-CoV-2 with fast and long-lasting immunity. *Acta Pharm Sin B* 2023;**13**:2219−33.
31. Islam MA, et al. Restoration of tumour-growth suppression *in vivo via* systemic nanoparticle-mediated delivery of PTEN mRNA. *Nat Biomed Eng* 2018;**2**:850−64.
32. Zhang T, et al. A high-efficiency, low-toxicity, phospholipids-based phase separation gel for long-term delivery of peptides. *Biomaterials* 2015;**45**:1−9.
33. Zhang T, et al. Injectable and biodegradable phospholipid-based phase separation gel for sustained delivery of insulin. *Colloids Surf B Biointerfaces* 2019;**176**:194−201.
34. Wang Y, et al. Dendritic cell biology and its role in tumor immunotherapy. *J Hematol Oncol* 2020;**13**:107.
35. Postow MA, Sidlow R, Hellmann MD. Immune-related adverse events associated with immune checkpoint blockade. *N Engl J Med* 2018;**378**:158−68.
36. DiNardo CD, et al. 10-day decitabine with venetoclax for newly diagnosed intensive chemotherapy ineligible, and relapsed or refractory acute myeloid leukaemia: a single-centre, phase 2 trial. *Lancet Haematol* 2020;**7**:e724−36.
37. Xu YP, et al. Tumor suppressor TET2 promotes cancer immunity and immunotherapy efficacy. *J Clin Invest* 2019;**129**:4316−31.
38. Yang J, Nie J, Ma X, Wei Y, Peng Y, Wei X. Targeting PI3K in cancer: mechanisms and advances in clinical trials. *Mol Cancer* 2019;**18**:26.
39. Fruman DA, Rommel C. PI3K and cancer: lessons, challenges and opportunities. *Nat Rev Drug Discov* 2014;**13**:140−56.
40. Chu T, Wang Z, Pe'er D, Danko CG. Cell type and gene expression deconvolution with BayesPrism enables Bayesian integrative analysis across bulk and single-cell RNA sequencing in oncology. *Nat Can (Que)* 2022;**3**:505−17.
41. Matulonis UA, Sood AK, Fallowfield L, Howitt BE, Sehouli J, Karlan BY. Ovarian cancer. *Nat Rev Dis Prim* 2016;**2**:16061.
42. Rebello RJ, et al. Prostate cancer. *Nat Rev Dis Prim* 2021;**7**:9.
43. Siegel RL, Miller KD, Jemal A. Cancer statistics. *CA Cancer J Clin* 2020;**70**:7−30.